JOURNAL OF PROPULSION AND POWER
Vol. 24, No. 3, May–June 2008

Prediction of the Efficiency of Acoustic Damping Cavities

Geoffrey Searby*
Centre National de la Recherche Scientifique and Aix-Marseille Université, 13384 Marseille, France
and
Aurélie Nicole,† Mohammed Habiballah,‡ and Emmanuel Laroche†
ONERA, 92322 Chatillon, France

DOI: 10.2514/1.32325

In this paper, we first recall the classical results for the laminar dissipation of acoustic energy in the boundary layer of a forced resonator. We then show how this result can be used in conjunction with a Helmholtz solver to calculate the laminar damping of a cavity of arbitrary geometry. This approach is validated by unsteady numerical simulations in both simple and complex geometries. The examples are nonreacting, but the approach can easily be extended to accommodate strong temperature variations. Finally, we suggest and validate a strategy that can use the damping obtained from the Helmholtz solver to calculate an equivalent resistive boundary condition that can be used in unsteady-time-domain simulations.

Nomenclature

c	=	speed of sound, m s^{-1}
D_{th}	=	thermal diffusivity, m^2/s
E	=	energy, J
e	=	energy per unit surface area, J m^{-2}
k	=	acoustic wave number, m^{-1}
L	=	length of cavity or chamber, m
P	=	chamber pressure, Pa
Pr	=	Prandtl number, $\equiv \nu/D_{\text{th}}$
p	=	acoustic pressure, Pa
R	=	radius of cavity or chamber, m
$\mathcal{R}$	=	real part of impedance, kg m^{-2} s^{-1}
S	=	section of cavity or chamber, m^2
St_{ac}	=	acoustic Strouhal number, $\omega R/\hat{u}$
T	=	temperature, K
u	=	acoustic velocity, m s^{-1}
$\mathcal{X}$	=	imaginary part of impedance, kg m^{-2} s^{-1}
γ	=	ratio of specific heats,
δ_ν	=	viscous boundary-layer thickness, m
μ	=	shear viscosity, Pa s
ν	=	kinematic viscosity, m^2/s
ρ	=	density, kg m^{-3}
σ	=	damping rate, s^{-1}
ω	=	angular frequency, s^{-1}

Subscripts

0	=	initial or mean value
1	=	main cavity
2	=	damping cavity
ν	=	viscous contribution
th	=	thermal contribution

Received 24 May 2007; revision received 16 November 2007; accepted for publication 24 November 2007.

*Senior Scientist, Laboratory Institut de Recherche sur les Phénomènes Hors Equilibre, 49 rue Joliot-Curie.
†Research Scientist, 29 Avenue de la Division Leclerc, Boite Postal 72.
‡Director, Fundamental and Applied Energetics Department, 29 Avenue de la Division Leclerc, Boite Postal 72.

Introduction

HIGH-FREQUENCY instability in liquid-fueled rocket engines is still an open problem [1,2]. Various methods have been used to increase the dissipation rate of acoustic disturbances in rocket engine combustion chambers, with the objective of increasing the stability margin of the motors. Among the well-known damping devices are baffles, acoustic liners, and quarter-wave resonators. These devices are conceptually simple. Baffles are placed at the injector face and are intended to damp transverse modes. They have the disadvantage of being exposed to the combustion region and need to be cooled. Acoustic liners on the combustion chamber wall have broadband acoustic dissipation characteristics, but can also create serious problems with wall cooling. Quarter-wave cavities are known to efficiently increase the stability margin when placed close to the injection plate. However, these devices have a relatively narrow dissipation bandwidth, and each cavity needs to be tuned to a specific chamber resonance.

Numerical simulation of all the processes occurring in a rocket engine combustion chamber is beyond the power of present computing capabilities and will remain so for the foreseeable future. It is thus necessary to model the small-scale processes. One such process that needs to be modeled is the acoustic energy dissipation in damping cavities. One of the possible schemes to introduce the effect of damping cavities without excessive computing cost in unsteady simulations is to implement the cavity damping as a boundary condition in unsteady computations [3,4].

Two distinct damping mechanisms are associated with acoustic dampers. The first mechanism arises from viscous drag and heat transfer at the cavity walls. This is a linear mechanism, and the associated acoustic resistance is independent of the acoustic amplitude. This mechanism dominates at low acoustic amplitudes and it is important for the linear stability of propulsion devices. The second mechanism arises from the formation of vortex eddies at the exit from the damping cavity (and also internally in the case of a perforated liner or a Helmholtz cavity). This is a nonlinear mechanism, and the associated acoustic resistance increases with the velocity of the flow at the entrance to the cavity [3,5,6]. The latter mechanism dominates at high acoustic amplitudes and determines the dynamic stability characteristics. The relative contribution of these two mechanisms is described by the acoustic Strouhal number $St_{\text{ac}} = \omega R/\hat{u}$, where R is the radius of the cavity exit, and $\hat{u}$ is the amplitude of the acoustic velocity at the cavity exit [7]. For $St_{\text{ac}} \gg 1$, the viscous mechanisms dominate. Because the two mechanisms are physically independent, the associated acoustic resistances are additive, at least up to moderately nonlinear acoustic levels.

In this paper, we will be concerned only with the linear viscous and thermal damping, which was intentionally neglected in [3,6]. We first recall the classical results for laminar energy dissipation in the boundary layer of a forced resonator. We then show how this result can be used to calculate the laminar damping of a cavity with arbitrary geometry, with the help of a lightweight Helmholtz solver. We then validate this approach by performing unsteady numerical simulations in both simple and complex geometries. We show that the damping rate from simulation agrees with analytical predictions for a trivial cylindrical cavity. For complex geometries, the results from numerical simulation are in close agreement with the predictions of the Helmholtz solver; in fact, the small discrepancies can be attributed to the finite size of the mesh in the acoustic boundary layers of the numerical calculations. Finally, we suggest a strategy that can use the damping calculated from the Helmholtz solver to implement an equivalent resistive boundary condition.

Laminar Boundary-Layer Theory

The laminar damping of an acoustic cavity has two contributions: 1) damping through viscous stresses at the walls and 2) damping through thermal exchange at the walls.

Viscous and Thermal Losses

The viscous and thermal losses are diffusive and obey qualitatively identical laws. The viscous dissipation is proportional to the product of the velocity gradient at the wall and the shear viscosity. The viscous energy dissipation was first calculated by Stokes [8] and then extended by Kirchhoff [9,10] in 1868. The thermal dissipation is proportional to the product of the temperature gradient at the wall and the thermal conductivity. The thermal energy dissipation was first calculated by Nielsen [11] in 1949.

Viscous Losses

The viscous loss in an acoustic cavity was first calculated by Stokes [8] and extended by Kirchhoff [9,10] in 1868. Here, we will use the boundary-layer formulation given by Batchelor [12], along with the reasoning used by Lambert [13]. Similar formulations can be found in other standard textbooks [14,15]. We consider only the (quasi-) steady-state situation, in which any time variation of the amplitudes is on a timescale that is much longer than the acoustic period.

As a starting point, it is easier to treat the case of an oscillating wall in contact with a stationary fluid. The y coordinate is normal to the wall (see Fig. 1). Consider a plane infinite wall oscillating with velocity $u = \hat{u}_x \cos(\omega t)$ along the x axis in a plane parallel to itself. If the fluid velocity at infinity is zero and transient effects are neglected, then Batchelor [12] (p. 192, Eq. 4.3.16) shows that the unsteady velocity profile in the liquid is given by

$$u(y,t) = \hat{u}_x \exp\left(-\frac{y}{\delta_\nu}\right)\cos\left(\omega t - \frac{y}{\delta_\nu}\right) \tag{1}$$

where δ_ν is a measure of the thickness of the unsteady viscous boundary layer:

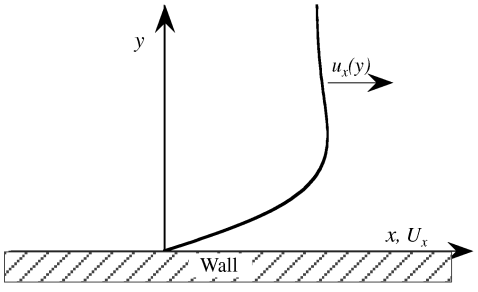

Fig. 1 Geometry for the calculation of velocity profile in an oscillating boundary layer.

$$\delta_\nu = \sqrt{\frac{2\nu}{\omega}} \tag{2}$$

where ν is the kinematic viscosity, and ω is the angular frequency. The velocity in the fluid oscillates with a wavelength $2\pi\sqrt{2\nu/\omega}$.

This result also applies to an acoustic boundary layer for the following reason: The preceding flow is a parallel shear flow, invariant by translation so that $\boldsymbol{u}\nabla\boldsymbol{u} = 0$, and Eq. (1) is a solution of the Navier–Stokes equation with constant pressure. The complementary situation, in which the plate is stationary but the main bulk of fluid oscillates, is obtained by a change of reference frame: $x' = x - (\hat{u}_x/\omega)\sin(\omega t)$. However, the only effect of this noninertial change of reference is to introduce an oscillating longitudinal pressure gradient $\partial p/\partial x = \omega\rho\hat{u}_x \sin(\omega t)$. It does not change the form of the solution for the velocity field:

$$u'(y,t) = \hat{u}_x\left[\exp\left(-\frac{y}{\delta_\nu}\right)\cos\left(\omega t - \frac{y}{\delta_\nu}\right) - \cos(\omega t)\right] \tag{3}$$

If the oscillations are produced by a plane acoustic wave, then the preceding argument remains valid, provided that $|\boldsymbol{u}\nabla\boldsymbol{u}|$ is negligible compared with $|\partial\boldsymbol{u}/\partial t|$ or, equivalently, $\hat{u}_x/c \ll 1$.

The force per unit area exerted by the wall on the liquid is given by $F = \mu(\partial u'/\partial y)|_{y=0}$ and so

$$F = \rho\nu\frac{\hat{u}_x}{\delta_\nu}(\sin(\omega t) - \cos(\omega t)) \tag{4}$$

Note that the force is *not* in phase with the wall velocity: there is a resistive (in-phase) component and a reactive (90-deg phase lag) component. Averaged over an acoustic period, only the resistive component contributes to the energy dissipated per unit area:

$$\left\langle\frac{\mathrm{d}e}{\mathrm{d}t}\right\rangle_\nu = \frac{1}{2}\rho\nu\frac{u_x^2}{\delta_\nu} \tag{5}$$

$$\left\langle\frac{\mathrm{d}e}{\mathrm{d}t}\right\rangle_\nu = \frac{1}{2}\rho u_x^2\sqrt{\frac{\omega\nu}{2}} \tag{6}$$

The total rate of energy dissipation in an acoustic cavity can then calculated by integrating Eq. (6) over all the solid walls:

$$\left\langle\frac{\mathrm{d}E}{\mathrm{d}t}\right\rangle = \int_S\left\langle\frac{\mathrm{d}e}{\mathrm{d}t}\right\rangle\mathrm{d}S \tag{7}$$

Thermal Losses

Acoustic oscillations are adiabatic if the wavelength λ satisfies $\lambda > 2\pi D_{\mathrm{th}}/c \approx 0.5\ \mu\mathrm{m}$, where D_{th} is the thermal diffusivity and c is the speed of sound. In combustion chambers, this inequality is always true, and so the acoustic pressure oscillations give rise to temperature oscillations:

$$\delta T = \frac{\gamma - 1}{\gamma}\frac{T_0}{P_0}p \tag{8}$$

where T_0 and P_0 are the average temperature and pressure, respectively; p is the oscillating acoustic pressure; $P = P_0 + p\sin(\omega t)$; and γ is the ratio of specific heats. In the presence of an isothermal wall there will be an oscillating heat flux to the wall. This heat flux is irreversible and contributes to energy dissipation. The calculation for the unsteady heat flux proceeds in a similar way to the calculation of the unsteady viscous stress and was calculated by Nielsen [11]. The final result [13] for the rate of energy loss per unit area is

$$\left\langle\frac{\mathrm{d}e}{\mathrm{d}t}\right\rangle_{\mathrm{th}} = \frac{1}{2}\frac{\gamma - 1}{\gamma}\frac{p^2}{P_0}\sqrt{\frac{\omega D_{\mathrm{th}}}{2}} \tag{9}$$

where D_{th} is the thermal diffusivity. For a perfect gas, the sound velocity is related to the mean pressure $P_0 \equiv (\rho c^2)/\gamma$, and in this case, Eq. (9) is easily written in a form that is symmetrical to Eq. (6):

$$\left\langle \frac{\mathrm{d}e}{\mathrm{d}t} \right\rangle_{\text{th}} = \frac{1}{2}(\gamma - 1)\frac{p^2}{\rho c^2}\sqrt{\frac{\omega D_{\text{th}}}{2}} \tag{10}$$

Application to a Cylindrical Resonator

Here, for illustration, we apply the preceding results to a cylindrical resonator that is closed at one or both ends. The cavity is directed along the x axis and is closed at $x = 0$. In the linear regime, the damping of acoustic energy is exponential

$$E(t) = E_0 \exp(-\sigma_E t)\exp(-\mathrm{i}\omega t)$$

and the damping rate σ_E is then given by

$$\sigma_E = \frac{1}{E}\frac{\mathrm{d}E}{\mathrm{d}t} \tag{11}$$

Note that the damping rate of the *pressure*, σ_p, is one-half of this quantity:

$$\sigma_p = \frac{1}{2E}\frac{\mathrm{d}E}{\mathrm{d}t} \tag{12}$$

In the preceding equations, E is the total energy in the cavity:

$$E = \frac{1}{T}\int_T \int_V \left(\frac{1}{2}\rho u^2(x,t) + \frac{1}{2}\frac{p^2(x,t)}{\rho c^2}\right)\mathrm{d}V\mathrm{d}t \tag{13}$$

The integration is over one period of oscillation, $T = 2\pi/\omega$, and over the volume of the cylinder, $\mathrm{d}V \equiv S\mathrm{d}x$. If the attenuation is weak, then the pressure and velocity in a standing wave can be written

$$\begin{aligned} p(x,t) &= \Re[\hat{p}\cos(kx)\exp(-\mathrm{i}\omega t)] \\ u(x,t) &= -\Im[\mathrm{i}\hat{u}\sin(kx)\exp(-\mathrm{i}\omega t)] \qquad \hat{p} = \rho c\hat{u} \end{aligned} \tag{14}$$

where $\hat{u}$ and $\hat{p}$ are the peak amplitudes of the velocity oscillations at the antinodes of velocity and pressure, respectively. They may be considered constant during a period of oscillation. The integral Eq. (13) is easily evaluated to give

$$E = \pi R^2 L\frac{1}{4}\rho\hat{u}^2 \equiv \pi R^2 L\frac{1}{4}\frac{\hat{p}^2}{\rho c^2} \tag{15}$$

This evaluation is correct for an arbitrary length of cylinder L, including nonresonant conditions.

Viscous Contribution

The viscous contribution to damping is given by the integral of Eq. (6) over the side walls of the cylinder. There is no contribution from the end walls, because the velocity there is zero.

$$\left\langle \frac{\mathrm{d}E}{\mathrm{d}t} \right\rangle_v = \pi RL\frac{1}{2}\rho\hat{u}^2\sqrt{\frac{\omega\nu}{2}}\left(1 - \frac{\sin(2kL)}{2kL}\right) \tag{16}$$

where $k \equiv \omega/c$ is the acoustic wave number. If the cylinder is resonant, then the term in kL disappears and the dissipation is maximal.

The viscous contribution to the damping rate, $\sigma_v \equiv (1/E)(\mathrm{d}E/\mathrm{d}t)_v$, is then

$$\sigma_v = \frac{2}{R}\sqrt{\frac{\omega\nu}{2}}\left(1 - \frac{\sin(2kL)}{2kL}\right) \tag{17}$$

Thermal Contribution

The thermal contribution to damping is given by the integral of Eq. (10) over the side walls of the cylinder. The integral must also be evaluated at the end wall(s) if the cylinder is closed, because these locations are antinodes for the oscillations of pressure and temperature:

$$\left\langle \frac{\mathrm{d}E}{\mathrm{d}t} \right\rangle_{\text{th}} = \pi RL(\gamma - 1)\frac{1}{2}\frac{\hat{p}^2}{\rho c^2}\sqrt{\frac{\omega D_{\text{th}}}{2}}\left(1 + \frac{\sin(2kL)}{2kL} + \frac{nR}{L}\right) \tag{18}$$

where n is the number of closed ends. If the cylinder is resonant, then the term in kL again disappears.

The thermal contribution to the damping rate, $\sigma_{\text{th}} \equiv (1/E)(\mathrm{d}E/\mathrm{d}t)_{\text{th}}$, is

$$\sigma_{\text{th}} = \frac{2(\gamma - 1)}{R}\sqrt{\frac{\omega D_{\text{th}}}{2}}\left(1 + \frac{\sin(2kL)}{2kL} + \frac{nR}{L}\right) \tag{19}$$

If the aspect ratio of the cylinder is high ($L \gg R$), then the contribution from the end wall(s) can be neglected.

Total Damping of a Cylindrical Resonator

The total damping rate is just the sum of the viscous and thermal contributions ($\sigma_e = \sigma_v + \sigma_{\text{th}}$):

$$\begin{aligned} \sigma_e = \frac{2}{R}\Bigg[&\sqrt{\frac{\omega\nu}{2}}\left(1 - \frac{\sin(2kL)}{2kL}\right) \\ &+ (\gamma - 1)\sqrt{\frac{\omega D_{\text{th}}}{2}}\left(1 + \frac{\sin(2kL)}{2kL} + \frac{nR}{L}\right)\Bigg] \end{aligned} \tag{20}$$

Equation (20) gives the damping rate of *energy* in the cavity. The damping rate of *pressure* is one-half of the damping rate of energy:

$$\begin{aligned} \sigma_p = \frac{1}{R}\sqrt{\frac{\omega\nu}{2}}\Bigg[&\left(1 - \frac{\sin(2kL)}{2kL}\right) \\ &+ \left(\frac{\gamma - 1}{\sqrt{Pr}}\right)\left(1 + \frac{\sin(2kL)}{2kL} + \frac{nR}{L}\right)\Bigg] \end{aligned} \tag{21}$$

where we expressed the thermal diffusivity in terms of the viscosity and the Prandtl number. Equivalent expressions have been obtained by other authors, such as Tijdeman [16], using a more rigorous formulation.

Numerical Applications

We performed a number of numerical simulations to confirm the preceding laminar boundary-layer theory and to validate the capacity of our code to correctly simulate acoustic waves and boundary-layer dissipation. We used the CEDRE code [17]. CEDRE is a multiphysics computational tool for numerical simulation in the field of energetics, with particular emphasis on propulsion applications. The code can handle coupled physical subsystems, each of them being taken into account by a specialized time-dependent solver:

1) The compressible flow module solves the Navier–Stokes equations with any number of species and various possible models for chemical reactions. The simulation space can be 3D or 2D (plane or axisymmetric). Several turbulence models are available, as well as large-eddy simulation.

2) Liquid and solid particles can be modeled in the Lagrangian or Eulerian approach, depending on the applications. In the two corresponding solvers, interactions with the gas include drag forces, heat exchanges, and vaporization–condensation. Different additional models for turbulent dispersion and fragmentation are available in the Lagrangian approach.

3) Radiation is calculated by a Lagrangian solver based on Monte Carlo methods.

4) For heat conduction in solid walls, an anisotropic solver with variable physical properties is currently under development.

For the simulations presented in this paper, the unsteady laminar viscous flow version of the code was used.

Table 1 Properties of gas used in simulations

Name	Value	Name	Value
T, K	2099	c, m/s	1884.5
ρ, kg/m^3	0.358	γ	1.27
μ, kg/m/s	4.833×10^{-5}	ν, m^2/s	1.35×10^{-4}
C_p, J/kg/K	6257.6	Pr	0.79

Table 2 Dimensions of the coupled cylinders

Name	Value	Name	Value
L_1	0.20 m	L_2	0.10 m
R_1	0.11 m	R_2	$7 \times 10^{-3} < R_2 < 20 \times 10^{-3}$ m

Validation on a Trivial Cylindrical Cavity

As a first check, we simulated a simple axisymmetric closed cavity of length $L = 0.5$ m and radius $R = 0.005$ m. The cylinder is filled with hot gas at 1 MPa, representative of the combustion products of a rich hydrogen–oxygen flame with a mixture ratio of 2:11. The physical properties of the mixture are given in Table 1.

The cylinder is meshed with 100 cells in the longitudinal direction. In the radial direction, the characteristic thickness of the acoustic boundary layer [Eq. (2)] is 152.7 μm. In a first simulation, we placed three cells of height 50 μm inside the boundary layer. Outside the boundary layer, the mesh size increases geometrically. The pressure distribution along the cylinder is initialized with the fundamental half-wavelength mode. In this simulation, the cavity walls were adiabatic, and so thermal losses do not contribute to the damping.

The damping rate was measured by fitting an exponentially decaying sinus to the pressure signal $p(t)$, recorded at one end of the cylinder. The pressure damping rate with the preceding mesh was $\sigma = 185.5$ s^{-1}. Decreasing the mesh size in the boundary layer from 50 to 23.8 μm and then to 7.55 μm decreased the measured damping rate to 179.4 s^{-1} and then to 178.5 s^{-1}, respectively. The theoretical damping rate according to Eq. (21) is 178.8 s^{-1}. This excellent agreement confirms both the validity of the laminar boundary-layer analysis and the capacity of the code to correctly handle viscous damping of acoustic waves.

Complex Axisymmetric Geometries

The application of Eqs. (6) and (10) to calculate the acoustic losses in a simple geometry is trivial. However, it is not possible to obtain an analytical expression for the acoustic field in an arbitrary geometry. Even for a relatively simple 2D axisymmetric geometry, such as that of the two coupled cylinders shown in Fig. 2, the analytical solution is not tractable.

To find the acoustic modes of an arbitrary geometry, we use COMSOL, a commercial solver, to resolve the Helmholtz equation for the acoustic pressure field:

$$\nabla^2\{c^2 p_n(\boldsymbol{x})\} + \omega_n^2 p_n(\boldsymbol{x}) = 0 \tag{22}$$

The eigenvalues ω_n are the resonant frequencies of the specified geometry, and c is the speed of sound, which is constant here, but may vary in space. Once the pressure field $p_n(\boldsymbol{x})$ at frequency ω_n is known, the acoustic velocity field can be calculated using momentum conservation in the frequency domain:

$$\mathrm{i}\,\omega_n \rho u_n(\boldsymbol{x}) + \nabla p_n(\boldsymbol{x}) = 0 \tag{23}$$

It should be noted that a resolution of the Helmholtz equation for a given geometry is a fast lightweight calculation compared with an unsteady resolution of the compressible Navier–Stokes equations. The solutions for the pressure field at frequencies ω_n can be used as initial conditions for a full unsteady simulation to investigate the behavior of a particular mode.

In these calculations, we do not consider the effects of a nonzero mean flow in the main combustion chamber: it would change the eigenfrequencies of the system. The effect is on the order of Mach^2 and is generally neglected. It is possible to calculate acoustic eigenvalues in the presence of a mean flow, but this is beyond the scope of the present paper. A mean flow will also modify the dissipation in the boundary layer; however, there is generally no mean flow in the damping cavities. In the main cavity, the magnitude of the effect depends not only on the Mach number of the mean flow, but also on the relative thickness of the acoustic and mean flow boundary layers. The latter is generally much larger, which decreases its influence.

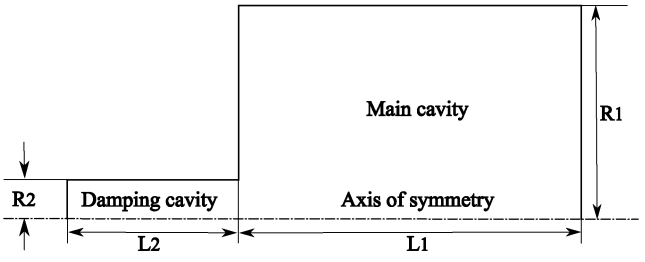

Fig. 2 Simple test case in which a main cylindrical cavity of length L_1 and radius R_1 is damped by a secondary cylindrical cavity of variable length and diameter.

Semi-Analytical Evaluation of the Damping Rate

Provided that the thickness of the boundary layer is small compared with the dimensions of the chamber, which is always the case for real systems, it is possible to evaluate the acoustic damping rate of the system from the Helmholtz solution for the pressure and velocity fields. The total energy in the acoustic field is found by integrating Eq. (13) over the volume of the geometry. The viscous and thermal loss rates in the boundary layers can be calculated by integrating Eqs. (6) and (10) over the rigid walls. The damping rate is then given by Eq. (12).

Comparison with the Results of Numerical Simulation

The damping rate of the axisymmetric geometry shown in Fig. 2 was obtained from numerical simulation using the CEDRE code, following the same procedure as for the trivial cylinder. The physical properties of the gas are the same as detailed previously (see Table 1), except for the viscosity, which was artificially increased by a factor 25, $\nu = 3.375 \times 10^{-3}$ m^2/s to reduce computing time. The dimensions of the test cases are summarized in Table 2. The length of the damping cavity was chosen to be one-half the length of the main cavity. This corresponds to the classical $\lambda/4$ tuning in which the length damping cavity is one-quarter wavelength at the fundamental frequency of the unperturbed main cavity.

The damping rates of the first two acoustic modes of the system at $f_1 \approx 4300$ Hz (mode 1) and $f_2 \approx 4800$ Hz (mode 2) were investigated. The exact frequencies of these two modes changes with the radius of the damping cavity, as shown in Fig. 3.

It may be noted that neither of these frequencies of this coupled system is equal to the resonant frequency of the unperturbed main

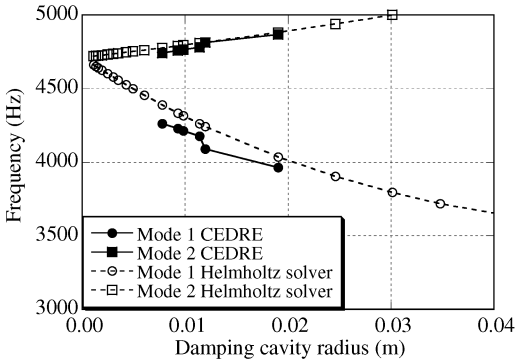

Fig. 3 Comparison of mode frequencies from the Helmholtz solver and from numerical simulation.

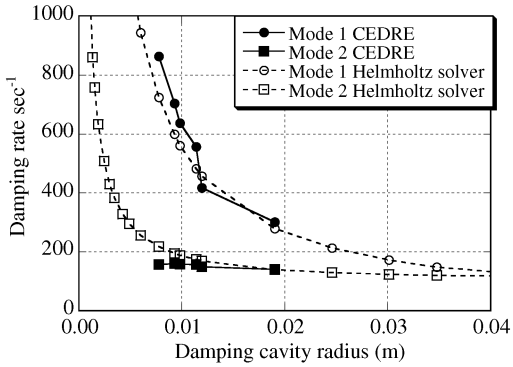

Fig. 4 Comparison of damping calculated from boundary-layer theory and damping from numerical simulation.

chamber, $f_0 = c/2L = 4710$ Hz. However, the frequencies of both modes tends to this limiting value as the radius of the damping cavity is decreased. The frequencies obtained from the numerical simulations agree well with the Helmholtz solver. The frequency of mode 1 from the numerical simulations is a little smaller than from the Helmholtz solver, because the latter does not take account of the frequency shift introduced by damping.

A comparison of the damping rates is shown in Fig. 4. Again the agreement between the results from numerical simulation and from the Helmholtz solver is good. The Helmholtz solver predicts that the total damping rate should increase as the radius of the damping cavity is decreased. The physical reason for this behavior is that the amplitude of the mode in the damping cavity increases as the radius of the cavity decreases, as illustrated by the ratio of the cavity end pressures in Fig. 5. Thus, the velocity gradient at the cavity walls increases as the cavity radius is decreased. This more than compensates the decrease in surface area at which dissipation occurs. Figure 5 also shows that the stronger damping of mode 1 arises from the fact that the acoustic pressure (and velocity) in the damping cavity is much higher for mode 1.

Of course, the damping rate cannot rise to infinity, and this prediction of the Helmholtz solver must break down at some minimum cavity radius. One obvious limit will arise when the thickness of the boundary layer is no longer negligible compared with the radius of the damping cavity. With the parameters used here, this will occur for a radius on the order of 0.002 m.

It is interesting to look at the details of the contribution of individual walls to the total damping, which is done in Fig. 6. The pressure fields for modes 1 and 2 are shown as backgrounds with the streamlines superimposed. The relative contribution to the total damping is shown against each wall. In these simulations, the cavity walls were adiabatic, and so there is no thermal damping. In this case, the end walls do not contribute to the damping because the velocity there is zero. For mode 1, 82% of the total damping is ensured by the damping cavity; nevertheless, 18% of the damping comes from the walls of the main chamber. For mode 2, the damping cavity is less efficient: only 54% of the total damping is provided by the damping cavity, and 46% comes from the walls of the main chamber.

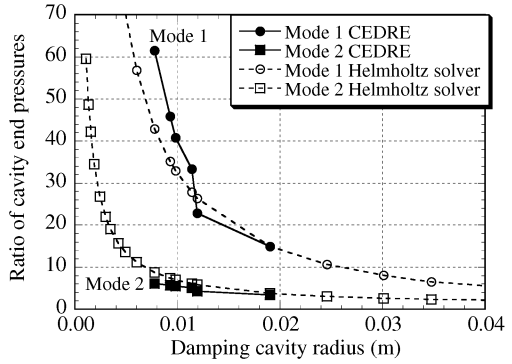

Fig. 5 Ratio of end pressure in the damping cavity to end pressure in the main chamber.

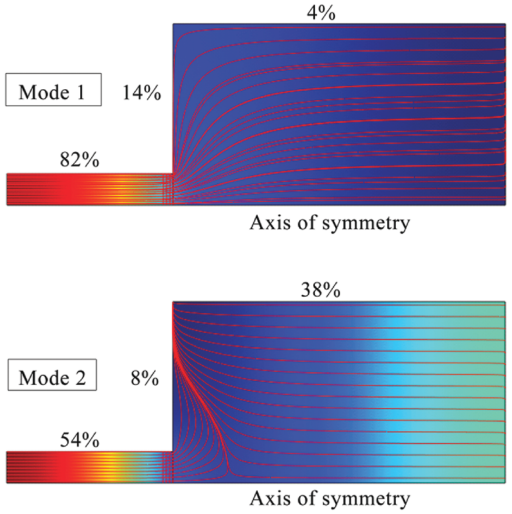

Fig. 6 Pressure field, streamlines, and relative contribution of walls to total damping. $R_2 = 0.019$ m.

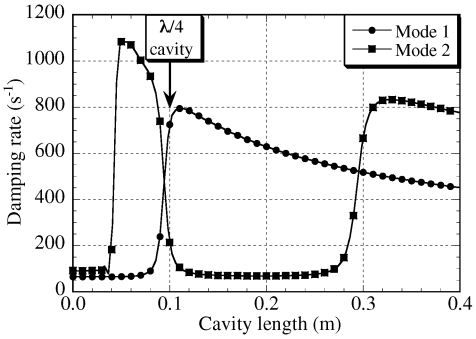

Fig. 7 Damping rate of modes 1 and 2 as a function of the length of the damping cavity; $R_2 = 0.0078$ m.

Finally, we investigate the relative damping of modes 1 and 2 as a function of the length of the damping cavity for a fixed cavity radius $R = 0.0078$ m. The results are plotted in Fig. 7. Only the results from the Helmholtz solver are shown. Numerical simulations of this aspect were not done. The maximum damping of mode 1 is obtained for a cavity length of 0.05 m ($\approx\lambda/8$ with respect to the first resonance of the unperturbed main chamber). The damping is then more than 10 times higher than that of the main chamber in the absence of the damping cavity. The maximum damping of mode 2 is obtained for a cavity length of 0.11 m ($\approx\lambda/3.6$ with respect to the first resonance of the unperturbed main chamber). Again, the total damping of this mode is more than 10 times higher than in the absence of the damping cavity. However, in the vicinity of the $\lambda/4$ tuning, the damping rates of both modes change very quickly with cavity length. This also means that the effective damping will be sensitive to small changes in local sound velocity in the main chamber. This will be the case in rocket engines in which there are temperature fluctuations and drifts linked to combustion processes. Finally, it can be seen that a reasonably good damping performance for both modes 1 and 2 can be obtained by detuning the damping cavity to a length greater than 0.31 m ($\gtrapprox\lambda/1.3$).

The numerical conclusions given in the preceding paragraph are specific to the particular model geometry of Fig. 2. However, we expect that the qualitative conclusions will remain valid for any geometry of a large chamber acoustically damped by one or more small cavities.

Nonaxisymmetric Geometries

We now look at the case of a nonaxisymmetric 2D geometry of a circular disk with a lateral rectangular damping cavity, illustrated in Fig. 8.

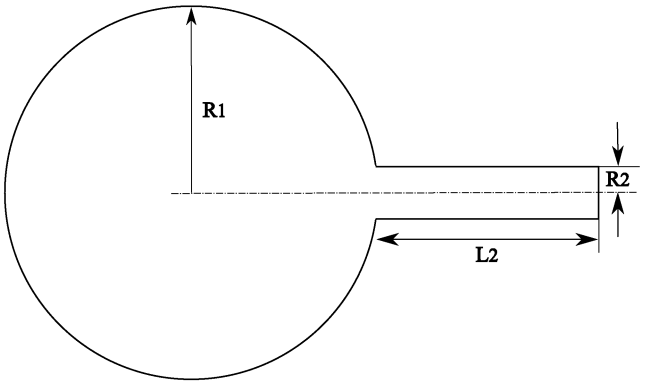

Fig. 8 Non axisymmetric geometry. A circular cavity of radius $R_1 = 0.1$ m is damped by a secondary rectangular cavity of length $L_2 = 0.041$ m and half-width $R_2 = 0.005$ m.

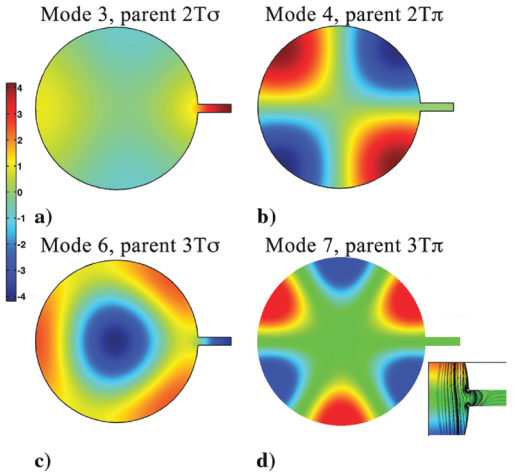

Fig. 9 Structure of modes 3, 4, 6, and 7. The inset shows the recirculation zones for mode 7 at the junction between the main and damping cavities.

Semi-Analytical Evaluations Using a Helmholtz Solver

The chamber is filled with a gas having the same physical properties given in Table 1, with the exception of the viscosity, which was increased tenfold ($\nu = 1.35 \times 10^{-3}$ m^2/s) to reduce computing time. The frequencies of the first seven resonant modes of this system and their damping rates, calculated by the Helmholtz solver, are listed in Table 3, along with values calculated by the CEDRE code (see the next section). The damping rates from the Helmhotz solver are in the laminar damping column. We classed the modes according to the parent mode. The parent mode is the corresponding mode of the disk when the length of the lateral cavity tends to zero. In this notation, T and R stand for tangential and radial parent modes, respectively. It should be noted that the actual mode geometry can change very rapidly as the length of the lateral cavity increases from zero [18,19], and a particular mode generally has neither a pure tangential nor a pure radial structure. For a given tangential parent mode (e.g., 2T) there are two daughter modes in the presence of the cavity (see Figs. 9a and 9b). The σ modes have an axis of symmetry aligned with the cavity. The structure and frequency of the σ modes depend strongly on the length of the cavity. The π modes have a pressure nodal line aligned with the cavity. The structure and frequency of the π modes are almost independent of the geometry of the cavity. By definition, the radial parent modes cannot have π daughter modes.

It can be seen from Table 3 that the damping rates of the π modes are small. This is to be expected, because the π modes do not excite significant flow in the damping cavity, and damping arises only from viscous dissipation at the walls of the main cavity. Modes 3 and 5 (parent modes 2Tσ and 1R) are strongly damped, However, mode 1 (parent mode 1Tσ) is only weakly damped; the lateral cavity is too short to be effective at the frequency of this mode. Rather surprisingly, mode 6 (parent mode 3Tσ) is also only weakly damped, although its frequency is close to the natural resonance of the lateral cavity. Some understanding can be gained by examining the structure shown in Fig. 9c. Although the parent of mode 6 is the 3Tσ mode of the circular cavity, due to the presence of the lateral cavity, the actual mode structure is a hybrid between radial and transverse. The attachment point is in a region of small pressure amplitude, close to a pressure node. Thus, the cavity is only weakly excited and the damping efficiency is low.

Comparison with the Results of CEDRE Numerical Simulation

The geometry is simulated using the CEDRE code. In the first series of simulations, the acoustic boundary layer is just resolved in the lateral damping chamber (two mesh points), but it is not resolved in the main chamber (mesh 1). This means that viscous dissipation at the walls of the main chamber is strongly underestimated. To simplify the posttreatment of the pressure signals, the initial pressure distribution in the simulation for each mode investigated was set equal to that computed by the Helmholtz solver. It was then found that the pressure decay remained monochromatic, confirming that the system was effectively initialized with a pure mode. The frequency and decay rate of each mode were found by fitting a decaying sinus to the pressure signal at one of the pressure sensors. A typical example is given in Fig. 10.

The damping rates obtained from these simulations are given in Table 3 in the CEDRE mesh 1 column. Only modes 3, 5, 6, and 7 were simulated. Modes 3 and 5 are found to be strongly damped, whereas modes 6 and 7 are only weakly damped, as predicted by the Helmholtz solver. However, the damping rates found for modes 3, 5, and 6 are approximately 15% higher than predicted, whereas the damping rate obtained for mode 7 is lower. In fact, the damping rate of mode 7 is underestimated by a factor that is close to two. The main reason for this lack of quantitative agreement is the poor resolution of the boundary layers in the numerical simulations.

We repeated the simulations using a refined mesh of 60 μm (mesh 2) at all the walls, including the main chamber. This puts three and four mesh points, respectively, in the boundary layers of modes 7 and 3. Because the computing time required with this mesh size is greatly increased, we simulated only these two modes. Mode 3 is a σ mode; its structure has a pressure gradient aligned with the damping cavity, as shown in Figure 9a. Mode 7 is the 3Tπ mode. It has the same structure as the 3T mode of a plain disk, with a pressure nodal

Table 3 Resonant frequencies and damping rates, calculated by the Helmholtz solver and from numerical simulation

Mode	Parent mode	Freq, Hz	Laminar damping s^{-1}	CEDRE mesh 1 s^{-1}	CEDRE mesh 2 s^{-1}
1	1Tσ	5378	30.1	——	——
2	1Tπ	5523	20.5	——	——
3	2Tσ	8449	203.2	240	220
4	2Tπ	9164	47.4	——	——
5	1R	10,177	297.3	341	——
6	3Tσ	11,600	33.4	37	——
7	3Tπ	12,607	77.0	39	83

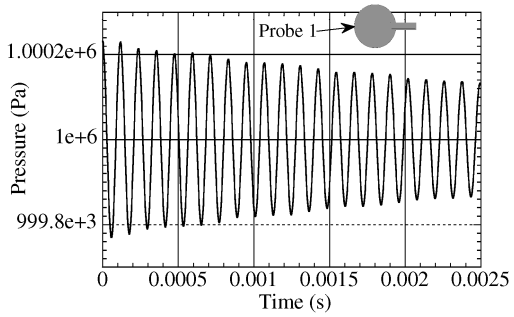

Fig. 10 Decaying pressure signal at the probe 1 position for mode 3.

line aligned with the damping cavity (see Fig. 9d). For this mode, the acoustic coupling with the cavity is almost negligible.

The damping rates obtained with this finer mesh are given in Table 3 in the CEDRE mesh 2 column. With this refined mesh, the damping rates from numerical simulations are closer to, but a little higher than, those predicted by the Helmholtz solver. The difference is approximately +7% for both modes. There are two possible origins for this residual discrepancy. First, all CFD codes introduce some internal numerical damping. Second, recirculation zones are generated by boundary-layer separation at the junction between the main chamber and the damping cavity. This is true even for the π mode 7, as can be seen in Fig. 9d. These recirculation zones dissipate energy and contribute to the acoustic damping. Because the Helmholtz solver solves only a potential problem, it cannot predict such recirculation zones. These two effects are sufficient to explain the slightly higher damping found by the CEDRE code, compared with the predictions of the Helmholtz solver.

Equivalent Resistance

In this section, we derive the equivalent acoustic resistance of a damping cavity and propose modeling strategy to use this resistance in numerical simulations.

Analytical Derivation

The acoustic impedance is defined by

$$Z = \frac{p}{u} \equiv \mathcal{R} + \mathrm{i}\mathcal{X}$$

The symbols $\mathcal{R}$ and $\mathcal{X}$ will be used to distinguish resistance $\mathcal{R}$ and reactance $\mathcal{X}$ from radius R and distance x.

Parameters and variables referring to the main cavity will be denoted by the subscript 1, and those referring to the damping cavity will be denoted by the subscript 2. We suppose that entrance to the cavity can characterized by an acoustic resistance $\mathcal{R}$. The power dissipated in this resistance is

$$\frac{\mathrm{d}E}{\mathrm{d}t} = \Re[p]\Re[u]S \tag{24}$$

where p and u are the pressure and velocity, and S is the area of entrance to the cavity. Substituting $p = Zu$ and taking the time average over one period of acoustic oscillation, we obtain

$$\left\langle \frac{\mathrm{d}E}{\mathrm{d}t} \right\rangle = \frac{1}{2}\mathcal{R}\hat{u}^2 S \tag{25}$$

If the cavity is excited at a frequency different from that of its natural resonance, the amplitude of the velocity $\hat{u}$ at the entrance is smaller than the amplitude $\hat{u}_0$ associated with the standing wave $u = \hat{u}_0 \sin(kL_2)\sin(\omega t)$.

The total acoustic energy inside the damping cavity is given by

$$E = \frac{1}{4}\rho_2 \hat{u}_0^2 S L_2 \equiv \frac{1}{4}\frac{\rho_2 \hat{u}^2 S L_2}{\sin^2(kL_2)} \tag{26}$$

where S is the area, as before, and L_2 is the length of the damping cavity. The intrinsic damping of the cavity is then

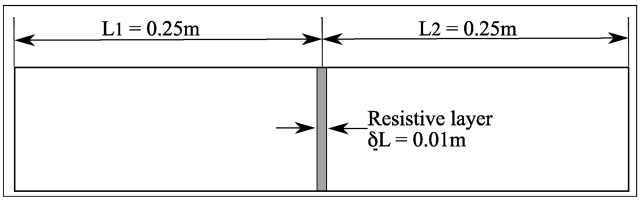

Fig. 11 Closed cavity with slip walls and a resistive layer.

$$\sigma_e = \frac{1}{E}\left\langle \frac{\mathrm{d}E}{\mathrm{d}t} \right\rangle = \frac{2\mathcal{R}}{\rho_2 L_2}\sin^2(kL_2) \tag{27}$$

Remember that this damping rate is that of *energy*, not of pressure.

We can now combine Eq. (27) with Eq. (20) to express the resistance at the cavity entrance in terms of the kinematic gas viscosity:

$$\mathcal{R} = \frac{\rho_2 L_2}{R_2 \sin^2(kL_2)}\sqrt{\frac{\omega\nu'}{2}} \tag{28}$$

We simplified the notation by writing

$$\nu' = \nu\left[1 - \frac{\sin(2kL_2)}{2kL_2} + \frac{\gamma - 1}{\sqrt{\mathrm{Pr}}}\left(1 + \frac{\sin(2kL_2)}{2kL_2} + \frac{R_2}{L_2}\right)\right]^2 \tag{29}$$

Equation (28) says that it is possible to replace the acoustic dissipation in the boundary layers of a damping cavity by placing an equivalent resistance at the entry to the cavity with slip wall conditions in the cavity. This can reduce computing time by a large factor.

Numerical Validation

We validated this approach for the trivial case of the previous cylindrical cavity of length $L = 0.5$ m, closed at both ends (see Fig. 11). In this case, the value of L_2 is one-half the length of the cylinder ($L_2 = 0.25$ m). However, because both half-cylinders contribute to the total damping, the value of resistance given by Eq. (28) must be doubled. Using the numerical values given in Table 1, the value of equivalent resistance is found to be

$$\mathcal{R} = 32.01 \text{ kg m}^{-2}\text{ s}^{-1} \tag{30}$$

The cylinder is regularly meshed with 100 cells in the longitudinal direction. The walls are adiabatic with a slip velocity condition. The resistance is inserted in the central region, two cells wide, by adding a term of the form $R\mathbf{u}/\delta L$ in the momentum equation, where δL (=0.01 m) is the length of the resistive zone. The calculation is initialized with the fundamental half-wavelength mode. The resulting evolution of the pressure at an end face is shown in Fig. 12. The acoustic frequency is 1884.1 Hz, as expected. The fitted damping rate is 178.53 s^{-1}. This value is very close to the theoretical value 178.80 s^{-1} predicted by Eq. (21). This excellent agreement validates the procedure and demonstrates that it is possible to model the acoustic damping effect of viscous boundary layers by introducing an equivalent resistance at the entry to damping cavities,

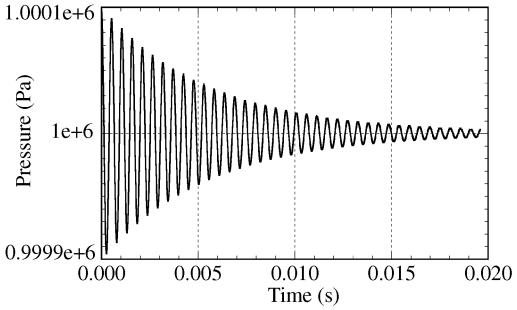

Fig. 12 Damping of a 0.5-m cavity with a central resistance 32.01 kg/m²/s.

which then need only to be coarsely meshed to capture the amplitude of the acoustic flowfield.

In principle, the equivalent resistance can be calculated from first principles using Eq. (28). However, in practice, it will be easier to use a Helmholtz solver to calculate the viscous energy dissipation rate dE/dt and the corresponding velocity amplitude at the cavity entrance and to then deduce the equivalent resistance from Eq. (25).

Conclusions

We used laminar boundary-layer theory to calculate acoustic energy dissipation in a damping cavity in the small-amplitude regime. The analytical result for the damping of a trivial cylindrical cavity was validated by numerical simulation. This theory can be used with a Helmholtz solver to calculate the linear damping of the acoustic modes of an arbitrarily complex geometry, provided that mean flow effects can be neglected. The calculation requires only a few seconds to a few minutes of processor time on a laptop computer. This approach was again validated by numerical simulation in two moderately complex geometries. Finally, we modeled the acoustic dissipation of damping cavities as a resistive layer at the entrance to the damping cavity. The value of the resistance is simply related to the calculated acoustic damping rate. The resistive layer was implemented in the unsteady CEDRE code by a local source term in the momentum conservation equation. This strategy introduces negligible computing overhead and eliminates the need to resolve the acoustic boundary layers. The performance on a trivial geometry is excellent. Work is under progress to test the strategy on more realistic configuration.

The cases considered here are all homogeneous. However, this is not a limitation and, in principle, the strategy is easily extended to reactive flows with large temperature gradients and/or variations in the composition of the gas, provided that they are known. In this context, it would be possible to couple the damping calculation from the Helmholtz solver with a time-dependent code to continuously evaluate and update the equivalent resistance in situations in which the gas properties (temperature, composition, and viscosity) evolve in time.

The only major drawback to this approach is that the equivalent resistance is a function of frequency. The resonant frequencies of the system are easily calculated using a Helmholtz solver. However, it is still necessary to have a priori knowledge concerning which mode is dominant in the system being simulated in the time-dependent code.

The strategy was tested in the zero-Mach-number approximation. The effect of finite Mach number of flow in the main chamber was not addressed and will certainly be more difficult to introduce in the model.

Although the underlying theory supposes potential acoustic flow and is thus limited to small-amplitude acoustics, we nevertheless anticipate that this approach will give good results up to moderately high acoustic levels. First, the acoustic boundary layers are always extremely thin compared with the dimensions of realistic rocket motors. Thus, we do not expect that large-scale flow turbulence can penetrate the acoustic boundary layers and modify the acoustic dissipation rate at the walls. Second, at moderate acoustic amplitudes, it is known that the acoustic dissipation rate is enhanced by boundary-layer separation with the subsequent formation of a jet at the cavity exit [5,6]. The acoustic energy used to form the jet is then dissipated by turbulence and/or by recirculation zones. This nonlinear dissipation mechanism occurs in parallel and independently of wall dissipation. Because we propose to maintain the geometrical presence of damping cavities in our strategy, the amplitude of the flow into and out of damping cavities should be correctly captured. Thus, the transfer of acoustic energy into jets should also be captured. Provided that the code dissipates the energy in these jets, it will also capture the basic nonlinearity of high-amplitude acoustic damping. The details of the model used to dissipate turbulent energy in the code are not important: the only requirement is that the energy in the jet be dissipated; that is, it is not restored back into the acoustic flow. Of course, these affirmations need to be validated by further work.

Acknowledgment

This work was supported by the Centre National d'Études Spatiales (CNES) in the framework of the French-German research program on rocket engine combustion stability.

References

[1] Harrje, D., and Reardon, F. (eds.), "Liquid Propellant Rocket Combustion Instability," NASA SP-194, Washington, DC, 1972.

[2] Yang, V., and Anderson, A., *Liquid Rocket Engine Combustion Instability*, Progress in Astronautics and Aeronautics, AIAA, Washington, DC, Vol. 169, 1995.

[3] Tang, P. K., and Sirignano, W. A., "Theory of a Generalized Helmholtz Resonator," *Journal of Sound and Vibration*, Vol. 26, No. 2, 1973, pp. 247–262. doi:10.1016/S0022-460X(73)80234-2

[4] Harrje, D., and Reardon, F. (eds.), "Liquid Propellant Rocket Combustion Instability," NASA SP-194, Washington, DC, 1972, pp. 138–159.

[5] Ingard, U., and Ising, H., "Acoustic Nonlinearity of an Orifice," *Journal of the Acoustical Society of America*, Vol. 42, No. 1, 1967, pp. 6–17. doi:10.1121/1.1910576

[6] Tang, P. K., Harrje, D. T., and Sirignano, W. A., "Experimental Verification of the Energy Dissipation Mechanism in Acoustic Dampers," *Journal of Sound and Vibration*, Vol. 26, No. 2, 1973, pp. 263–267. doi:10.1016/S0022-460X(73)80235-4

[7] Peters, M., Hirschberg, A., Reijnen, A., and Wijnands, A., "Damping and Reflection Coefficient Measurements for an Open Pipe at Low Mach and Low Helmholtz Numbers," *Journal of Fluid Mechanics*, Vol. 256, 1993, pp. 499–534. doi:10.1017/S0022112093002861

[8] Stokes, G. G., "On the Communication of Vibration from a Vibrating Body to a Surrounding Gas," *Philosophical Transactions of the Royal Society of London*, Vol. 158, 1868, pp. 447–463. doi:10.1098/rstl.1868.0017

[9] Kirchhoff, G., "Ueber den Einfluss der Wärmeleitung in Einem Gase auf die Schallbewegung," *Annalen der Physik und Chemie*, Vol. 210, 1868, pp. 177–193. doi:10.1002/andp.18682100602

[10] Kirchhoff, G., "On the Influence of Heat Conduction in a Gas on Sound Propagation," *Benchmark Papers in Acoustics, 4: Physical Acoustics*, edited by R. Lindsay, Dowden, Hutchison and Ross, Stroudsberg, PA, 1974.

[11] Nielsen, A. K., "Acoustic Resonators of Circular Cross-Section and with Axial Symmetry," *Transactions of the Danish Academy of Technical Sciences*, Vol. 10, Danish Academy of Technical Sciences, Copenhagen, 1949, pp. 9–70.

[12] Batchelor, G., *An Introduction to Fluid Dynamics*, Cambridge Univ. Press, New York, 1967.

[13] Lambert, R., "A Study of the Factors Influencing the Damping of an Acoustical Cavity Resonator," *Journal of the Acoustical Society of America*, Vol. 25, No. 6, 1953, pp. 1068–1083.

[14] Rayleigh, J., *The Theory of Sound*, Dover, New York, Vol. 2, 1945.

[15] Landau, L., and Lifchitz, E., *Fluid Mechanics*, 1st ed., Pergamon, New York, 1986.

[16] Tijdeman, H., "On the Propagation of Sound Waves in Cylindrical Tubes," *Journal of Sound and Vibration*, Vol. 39, No. 1, Mar. 1975, pp. 1–33. doi:10.1016/S0022-460X(75)80206-9

[17] Chevalier, P., Courbet, B., Dutoya, D., Klotz, P., Ruiz, E., Troyes, J., and Villedieu, P., "CEDRE: Development and Validation of a Multiphysics Computational Software," 1st European Conference for Aerospace Sciences (EUCASS), Moscow, http://cedre.onera.fr/publications/pdf/chevalier_EUCASS_2005.pdf.

[18] Cheuret, F., "Instabilités Thermo-Acoustiques Hautes-Fréquence Dans les Moteurs Fusées," Ph.D. Thesis, Univ. d'Aix-Marseille I, Marseille, France, Oct. 2005, http://tel.archives-ouvertes.fr/tel-00011656.

[19] Oschwald, M., Faragó, Z., Searby, G., and Cheuret, F., "Resonance Frequencies and Damping of a Cylindrical Combustor Acoustically Coupled to an Absorber," *Journal of Propulsion and Power*, Vol. 24, No. 3, 2008, pp. 524–533. doi:10.2514/1.32313

D. Talley
Associate Editor